Signal, Image and Video Processing
https://doi.org/10.1007/s11760-018-1274-0

ORIGINAL PAPER

A non-rigid image registration method based on multi-level B-spline and L2-regularization

Huizhong Ji[1] · Yusen Li[1] · Enqing Dong[1] · Peng Xue[1] · Wenshuo Xiong[1] · Wenyan Sun[1] · Zhenchao Tang[1] · Dejing Zhang[1] · Wei Fang[2]

Received: 23 June 2017 / Revised: 8 March 2018 / Accepted: 9 March 2018

Abstract
To solve the problem that the cost function of the classic free-form deformation (FFD) cannot simulate transformation field of images with large elastic deformation or local distortion in image registration better, and to increase the registration accuracy and robustness, a new non-rigid image registration method based on the classic hierarchical FFD is proposed. Since the smooth term has a significant influence on registration accuracy, and its coefficient is not easy to be controlled in the classic hierarchical B-spline based FFD, a L2-regularization term with faster and more stable optimization is introduced in the cost function of the proposed model. By coordinating the coefficients of this regularization term and the smooth term, this novel L2-regularized FFD model is able to solve the problem of low registration accuracy caused by strong smooth constraint while maintaining the images topologies. The introduced L2-regularization term can impose a spatial constraint on the control lattices transformation field, and the over-registration problem can be suppressed to a certain extent, so it can register the images with local large distortion. A series of registration experiments of natural images and medical images show that the new method has an obvious advantage over the classic model in registration accuracy measured by mean square error.

Keywords Non-rigid image registration · B-spline · Free-form deformation · L2-norm

1 Introduction

Image registration is a hot topic in image processing and has been widely used in many fields, such as cartography, medical image analysis and computer vision [1]. At present, there are multiple categories of image registration methods. The most common is based on the feature spaces. According to the different feature spaces, registration methods can be divided into two types: feature-based registration and pixel-based registration.

The feature-based registration, such as SIFT (scale-invariant feature transform) [2], ICP (iterative closest point) [3] and SURF (speeded up robust features) [4], is efficient in general. However, due to the part of the extracted image information used, these methods cannot provide reliable information in images, and registration accuracy, and robustness will be affected.

In pixel-based methods, physical model-based methods, such as linear elastic model, viscous fluid model and optical flow model, are frequently used. Thirion [5] proposed the classic Demons registration method based on optical flow model in 1998. Later, the researchers improved the Demons method for accuracy and efficiency, such as Active Demons [6], Multi-scale Implementation Active Demons (MIAD) [7] and SIFT-Demons [8]. Pock and Urschler [9] proposed a TV-L1 algorithm based on the optical flow field model in 2007, which provides a accurate registration result.

Thin plate spline [10] and the B-spline-based free-form deformation registration method [11] belong to linear elastic model, but the former cannot handle the local transformation as good as the latter. Rueckert et al. [11] were the first researchers to introduce the B-spline method, for sampling [12,13], into image registration. They applied the uniform multi-level B-spline method proposed by Lee and Wolberg

Huizhong Ji and Yusen Li have been contributed equally to this work.

✉ Enqing Dong
enqdong@sdu.edu.cn

✉ Dejing Zhang
dejingzhang@sdu.edu.cn

[1] School of Mechanical, Electrical and Information Engineering, Shandong University, Weihai, China

[2] Department of CT-MRI, Yidu Central Hosptial of Weifang Medical College, Shandong, Qingzhou, China

Published online: 17 March 2018

[14] for scattered data interpolation [15] to the non-rigid registration of breast MRI, and obtained good results. Some of the follow-up methods were mainly based on certain improvements in this method. For example, Schnabel and Rueckert [16] proposed a non-uniform multi-level FFD to improve the efficiency. Oliveira et al. [17] introduced an enhanced B-spline methodology to align plantar pressure image sequences simultaneously in time and space.

Although the classic FFD registration method based on uniform B-spline can achieve good results [11], it is hard to get accurate results in the images with both large local deformation and global deformation [16]. When the smooth term in cost function is relatively large, the accuracy is low. While the smoothing term is too small or nearly to 0, an over-registration occurs, and the image topologies will be destroyed. Therefore, there are always some areas which cannot be registered accurately. In this paper, we propose a multi-level B-spline-based FFD for non-rigid image registration by introducing a L2-regularization term, which can check and balance the effect of the smooth term and improves the registration accuracy. In addition, the L2-norm can well avoid over-fitting and reducing the errors, so that the topologies can be maintained and the robustness is enhanced.

2 Classic FFD based on multi-level B-spline

2.1 The Classic Hierarchical FFD Model

The images to be registered can be either natural images or medical images. Under normal situation, there are both rigid transformation and non-rigid transformation among them. Therefore, the transformation model is divided into two parts, namely global transformation and local transformation. Assuming the global transformation is T_{global} and the local transformation is T_{local}, then the total transformation T is:

$$T(x, y) = T_{\text{global}}(x, y) + T_{\text{local}}(x, y) \tag{1}$$

(1) Global Transformation: For 2D image *I(x,y)*, the global transformation uses an affine transformation with 6 degrees of freedom to describe the rigid transformation between the two images, such as rotation and zooming. The transformation function can be written as:

$$T_{\text{global}}(x, y) = \begin{pmatrix} \theta_{11} & \theta_{12} \\ \theta_{21} & \theta_{22} \end{pmatrix} \begin{pmatrix} x \\ y \end{pmatrix} + \begin{pmatrix} \theta_{13} \\ \theta_{23} \end{pmatrix} \tag{2}$$

The set Θ consisting of 6 elements $\theta_{11}, \theta_{12}, \ldots, \theta_{23}$ is the coefficient matrix of the affine transformation, which parameterizes the transformation model. For 3D image *I(x,y,z)*, the coefficient matrix has 12 elements, so the affine transformation has 12 degrees of freedom. The transformation function can be written as:

$$T_{\text{global}}(x, y, z) = \begin{pmatrix} \theta_{11} & \theta_{12} & \theta_{13} \\ \theta_{21} & \theta_{22} & \theta_{23} \\ \theta_{31} & \theta_{32} & \theta_{33} \end{pmatrix} \begin{pmatrix} x \\ y \\ z \end{pmatrix} + \begin{pmatrix} \theta_{14} \\ \theta_{24} \\ \theta_{34} \end{pmatrix} \tag{3}$$

(2) Local Transformation: Affine transformation can only describe the global rigid deformation of an image, therefore we need to use other methods to describe the local non-rigid deformation. The classic FFD based on multi-level B-spline has been proved a powerful tool for describing local deformation [18]. The basic principle of FFD is to simulate the transformation by manipulating the control grid covering the image. For a 2D image, assuming a uniform control grid with a resolution of $n_x \times n_y$ is provided, and a B-spline-based FFD can be written as:

$$T_{\text{local}}(x, y) = \sum_{k=0}^{3} \sum_{l=0}^{3} B_k(s) B_l(t) \phi_{(i+k)(j+l)} \tag{4}$$

where $i = \lfloor x/n_x \rfloor - 1$, $j = y/n_y \rfloor - 1$, $s = x/n_x - \lfloor x/n_x \rfloor$, $t = y/n_y - \lfloor y/n_y \rfloor$ and, for u∈[0,1)

$$\begin{cases} B_0(u) = (1-u)^3/6, \quad B_1(u) = (3u^3 - 6u^2 + 4)/6 \\ B_2(u) = (-3u^3 + 3u^2 + 3u + 1)/6, \quad B_3(u) = u^3/6 \end{cases} \tag{5}$$

This model can also be expressed in matrix form. Assuming the transformation model is $\boldsymbol{D}$, the control point matrix is $\boldsymbol{\Psi}$, and the constant matrix is $\boldsymbol{M}$, then Eq. (4) can be expressed as:

$$\boldsymbol{D} = \begin{bmatrix} s^3 & s^2 & s & 1 \end{bmatrix} \boldsymbol{M} \boldsymbol{\Psi} \boldsymbol{M}^{\mathrm{T}} \begin{bmatrix} t^3 & t^2 & t & 1 \end{bmatrix}^{\mathrm{T}} \tag{6}$$

where

$$\boldsymbol{M} = \frac{1}{6} \begin{bmatrix} -1 & 3 & -3 & 1 \\ 3 & -6 & 3 & 0 \\ -3 & 0 & 3 & 0 \\ 1 & 4 & 1 & 0 \end{bmatrix}, \quad \boldsymbol{\Psi} = \begin{bmatrix} \phi_{ij} & \cdots & \phi_{i(j+3)} \\ \vdots & \ddots & \vdots \\ \phi_{(i+3)j} & \cdots & \phi_{(i+3)(j+3)} \end{bmatrix} \tag{7}$$

B-spline has a good property of controlling local transformation, when a control point changes, only affecting the transformation in its neighborhood. We choose the multi-level B-spline as the transformation model, and select appropriate hierarchical grades for non-rigid registration.

Let $\Phi_1, \Phi_2, \ldots, \Phi_L$ denote the B-spline control grids from the first level to the Lth level, and the grid resolution is increasing by 2 times. Each level of control grid Φ_p defines a local transformation function T^p_{local} of this level, and its expression is given by Eq. (13). Therefore, the local transformation model $T_{\text{local}}(x, y)$ based on the multi-level B-spline can be written as:

$$T_{\text{local}}(x, y) = \sum_{p=1}^{L} T^p_{\text{local}}(x, y) \tag{8}$$

According to Eq. (6), Eq. (8) can also be expressed in matrix form. If the transformation model is $\boldsymbol{D}_{\text{local}}$ and the pth control point matrix is $\boldsymbol{\Psi}_p$, then Eq. (8) can be expressed as:

$$\boldsymbol{D}_{\text{local}} = \begin{bmatrix} s^3 & s^2 & s & 1 \end{bmatrix} \boldsymbol{M} \left(\sum_{p=1}^{L} \Psi_p \right) \boldsymbol{M}^{\mathrm{T}} \begin{bmatrix} t^3 & t^2 & t & 1 \end{bmatrix}^{\mathrm{T}} \tag{9}$$

In this way, local transformations are described by a series of hierarchical B-spline-based FFD models from coarse to fine, as shown in Eqs. (8) and (9).

2.2 Cost function of the classic FFD method

From Eq. (10), we can see that the registration transformation T is composed of global rigid transformation and local non-rigid transformation. Let $I(x,y)$ be the moving image, and $I(x_o, y_o)$ be the fixed image, then the cost function can be written as:

$$C = C_{\text{similarity}}(I(x_o, y_o), T(I(x, y))) + \lambda C_{\text{smooth}}(T) \tag{10}$$

$C_{\text{similarity}}$ is the similarity measure. For the single-mode images, to reduce the complexity, we choose the sum of squared differences (SSD) or the sum of absolute differences (SAD) as the similarity measure.

C_{smooth} is the smooth constraint term, and the coefficient λ is used to adjust its weight in the formula. In 2D images, this term is expressed as:

$$C_{\text{smooth}} = \frac{1}{\Omega} \int_0^X \int_0^Y \left(\frac{\partial^2 T}{\partial x^2} \right)^2 + \left(\frac{\partial^2 T}{\partial y^2} \right)^2 + 2 \left(\frac{\partial^2 T}{\partial xy} \right)^2 dx\, dy. \tag{11}$$

where Ω represents the area of the image domain. Correspondingly, the expression in 3D images is:

$$C_{\text{smooth}} = \frac{1}{V} \int_0^X \int_0^Y \int_0^Z \left(\frac{\partial^2 T}{\partial x^2} \right)^2 + \left(\frac{\partial^2 T}{\partial y^2} \right)^2 + \left(\frac{\partial^2 T}{\partial z^2} \right)^2 + 2 \left(\frac{\partial^2 T}{\partial xy} \right)^2 + 2 \left(\frac{\partial^2 T}{\partial yz} \right)^2 + 2 \left(\frac{\partial^2 T}{\partial zx} \right)^2 dx\, dy\, dz. \tag{12}$$

where V represents the volume of the image domain.

The smooth constraint only works on local non-rigid transformation and has no effect on global affine transformation.

3 LFFD model for registration

3.1 Limitation of the Classic FFD Method

The classic FFD method has been proved reliable to a certain extent, but it still has an obvious limitation. Through a large number of experiments, it has been found that this method cannot deal with the images with large local deformation or large distortion, and cannot simulate the transformation field well, so it cannot to get more accurate results. The limitation of the classic FFD method will be explained in detail by a set of experimental results shown as follows.

Figure 1a, b shows the moving image and fixed image of the liver MRI with a size of 256 × 256. Figure 1c is the registration result of the classic FFD method, and its corresponding parameters are set as follows: SAD is used as similarity measure, number of B-spline levels is 3, the initial control point spacing is 32×32, the coefficient λ is set to 0.01. Figure 1d shows the initial difference image between the moving image and fixed image. Figure 1e shows the difference image between the registration result and fixed image.

From the registration results, we can see that the classic FFD performs well in the global non-rigid transformation, but bad in the local transformation. The red circles in the liver images highlight the region with large deformation, and the structure in the circles is extremely irregular in shape. By observing the two difference images, we can conclude that the result obtained by the classic FFD is barely satisfactory, and there is a large room for improvement in the local transformation.

In the above experiments which were tested with different values of λ, we conclude that when λ=0.01, we can get the best result. However, the best result is not satisfactory enough, in fact, the problem is exactly in the smooth term. Smooth term can be weighted with λ, but when λ is too small or taken as 0, it is possible to make transformation field fold. And for a large value of λ, the smooth constraint is too strong, resulting in decreased accuracy. Taking a compromise value of λ, we can only get a compromise effect, just like Fig. 1c shows. This is the main reason why less methods are pro-

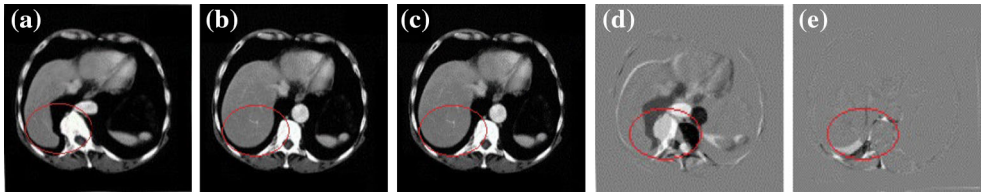

Fig. 1 Registration results of liver MRI using classic hierarchical FFD. **a** Moving image, **b** fixed image, **c** registration result, **d** initial difference, **e** resulting difference

posed to improve the accuracy of FFD compared to Demons [5–8] and optical flow [9,19].

3.2 LFFD model and analysis

Assuming vector $\boldsymbol{V}=[v_1, v_2, \ldots, v_n]$ is an n-dimensional vector, then the L2-norm of vector $\boldsymbol{V}$ is defined as:

$$\|\boldsymbol{V}\|_2 = \left(\sum_{i=1}^{n} (v_i)^2\right)^{\frac{1}{2}} \tag{13}$$

Assuming $\boldsymbol{U}$ is a matrix with m rows and n columns, u_{ij} denotes the value of element located at ith column jth row, then the Frobenius norm of matrix $\boldsymbol{U}$ is defined as:

$$\|\boldsymbol{U}\|_F = \left(\sum_{i=1}^{m}\sum_{j=1}^{n} \left(u_{ij}\right)^2\right)^{\frac{1}{2}} \tag{14}$$

In machine learning, Lp-norm is always used for better optimization, for example, L1-norm is usually used in sparse representation for feature selection [20]. L2-norm has the good property of preventing over-fitting, reducing the error, making the optimization fast and stable, and imposing spatial constraints on the model. Therefore, it is a common optimization method for the optimized model to introduce the L2-norm [18].

For the cost function of the classic FFD method shown in Eq. (10). To ensure the registration accuracy and balance the effect of the smooth constraint, we attempt to improve the classic model as follows:

$$\begin{aligned}\arg\min_{\Psi} \boldsymbol{E}(\Psi) =& C_{\text{similarity}}(I(x_o, y_o), T(I(x, y))) \\ &+ \lambda_L \|\Psi\|_F + \lambda_R C_{\text{smooth}}(T)\end{aligned} \tag{15}$$

where Ψ is the introduced L2 term, and λ_L is the coefficient for controlling the L2 item in the cost function. $C_{\text{smooth}}(T)$ is the smooth constraint term, of which λ_R is the weight coefficient.

After analyzing the shortcomings of the classic FFD, it can be seen that the classic FFD model cannot achieve the accurate registration due to the effect of the smooth term which should not be too small neither too heavy. The L2 term is introduced to check and balance the smooth constraint term. If we minimize $\|\Psi\|_F$, we can make every element of Ψ as small as possible, so we can limit the B-spline control point as much as possible. Reasonable displacement can play the role of maintaining the image topologies. By coordinating the coefficients of this regularization term and the smooth term, theoretically it is able to solve the problem of low registration accuracy caused by strong smooth constraint while maintaining the topologies.

3.3 LFFD model validity check

In this section, we chose checkboard synthetic image to check the validity of the LFFD method. Distort the image in advance, and then registered it with the original checkboard image.

Analyzing the effect of smooth term, the experimental scenario is designed as two situations. Situation 1: the smooth coefficient of the classic FFD is set properly to obtain the best result, then, the L2 term of the control points matrix is introduced, and finally, we compare and analyze the registration results. Situation 2: the smooth term coefficient is 0, and only the similarity measure is used, then the L2 term is introduced, and finally get the results.

Based on the above, the parameters are set as follows: SAD used as similarity measure, the B-spline levels is 3, and initial control points spacing is 32×32. The above parameters are fixed. For situation 1, the smooth term coefficient of classic FFD is set to $\lambda = 10^{-3}$, while in the LFFD, $\lambda_R = 10^{-3}$, and the coefficient of L2-norm is set to $\lambda_L = 3 \times 10^{-4}$. For situation 2, the smooth term coefficient of classic FFD is set to $\lambda = 0$, while in the LFFD, $\lambda_R = 0$, and the coefficient of L2-norm is set to $\lambda_L = 3 \times 10^{-4}$. So that we can check its validity.

Figure 2c–f shows the results of the four experiments. Figure 3a is the initial difference image, and Fig. 3b–e shows the difference between the fixed image and the registration results of four experiments. Figure 4a–d shows the transformation fields of the first level of B-spline control grids in four experiments. Figure 4e–h shows the second level correspondingly. Figure 4i–l shows the third level. Table 1 shows the objective evaluation criteria.

To see from Figs. 2, 3 and 4, the classic FFD method can maintain the image topologies only when the smooth-

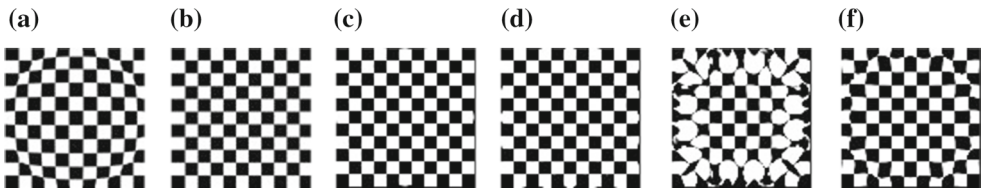

Fig. 2 Registration results of checkboard image. **a** Moving image, **b** fixed image, **c** $\lambda = 10^{-3}$, **d** $\lambda_L = 3 \times 10^{-4}, \lambda_R = 10^{-3}$, **e** λ=0, **f** $\lambda_L = 3 \times 10^{-4}, \lambda_R = 0$

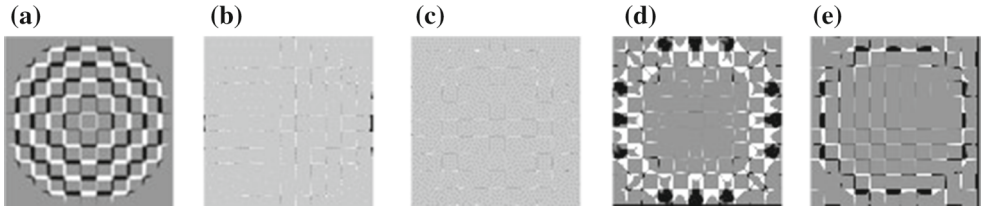

Fig. 3 Difference images. **a** Initial difference, **b** $\lambda = 10^{-3}$, **c** $\lambda_L = 3 \times 10^{-4}, \lambda_R = 10^{-3}$, **d** $\lambda = 0$, **e** $\lambda_L = 3 \times 10^{-4}, \lambda_R = 0$

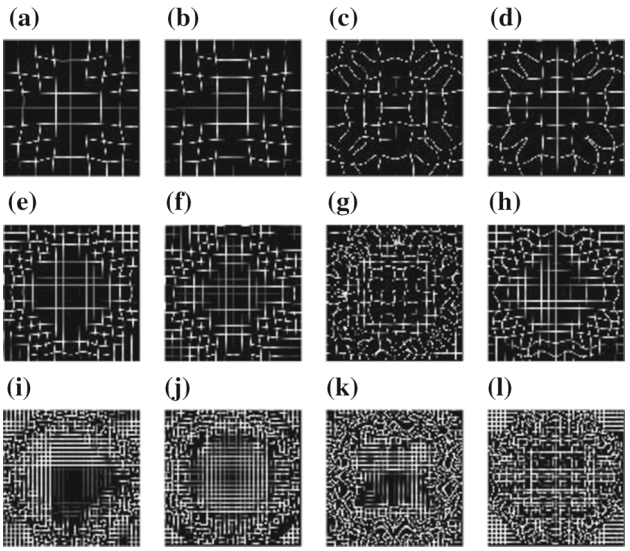

Fig. 4 Three levels of control points transformation fields for checkboard image. **a**–**d** are the first level transformation fields of control grid: **a** FFD with $\lambda = 10^{-3}$, **b** LFFD with $\lambda_L = 3 \times 10^{-4}, \lambda_R = 10^{-3}$, **c** FFD with $\lambda = 0$, **d** LFFD with $\lambda_L = 3 \times 10^{-4}, \lambda_R = 0$. **e**–**h** and **i** to **l** are the second and third level transformation fields of control grid correspondingly

ing constraint is relatively strong. When the smooth term is 0, due to the large spacing, the transformation field of the first level does not fold, while the second and third levels fold seriously. With the damaged topologies, the registration results are unreliable. After introducing the L2 term, using the same smoothing parameter, it can effectively restrain the over-registration. The second and third level do not fold, and the topologies maintained, so convictive to prove the validity.

Combining Figs. 2, 3 and 4 and Table 1, we find that the classic FFD can achieve good results when the smooth constraint is relatively strong. Based on this, we introduce L2 term, which can fine-tune the registration result and has an improvement in accuracy. Since the L2 term can impose a spatial constraint on the model, so this term makes those transformed control points reduce the displacement that should not be produced, thus increasing the registration accuracy.

Table 1 shows that LFFD has obvious advantages over the classic FFD on the mean square error. Therefore, we can roughly conclude that the result can be better after introducing the L2 term under these situations. When the smooth term is 0, the checkboard image will be seriously over-registered, the topologies destroyed, making results completely unreliable. If the L2 term is introduced under this situation, it can suppress the irrational spatial transformation of control grids, thus ensuring the topologies without distortion.

After the subjective and objective analysis of the above image registration experiment results, it is proved that the L2 term can better maintain the topologies of the images with the obvious distorted regions such as checkboard. At the same time, the proposed new method has a certain improvement in the accuracy compared with the classic FFD method.

3.4 Implementation steps of LFFD

Because of the numerous datum to be optimized in experiment, L-BFGS algorithm is chosen for the LFFD method, which is an improvement based on the BFGS algorithm. It solves the problem that require a lot of memory in the BFGS algorithm. The detailed description of implementation can be seen in Table 2.

4 Classic FFD based on multi-level B-spline

To verify the practical effect of the proposed method, natural images and medical images are used for experiments.

Table 1 The objective evaluation criteria

Parameters	PSNR (dB)	MSE (10^{-3})	R_{cc} (10^{-2})	MI	SSIM (%)
Before registration	54.90	210.8	56.95	0.20	37.17
$\lambda = 10^{-3}$	72.72	3.5	98.32	0.70	96.66
$\lambda_L = 3 \times 10^{-4}, \lambda_R = 10^{-3}$	**76.37**	**1.5**	**99.70**	**0.70**	**98.97**
$\lambda = 0$	56.90	132.1	0.72	0.31	51.66
$\lambda_L = 3 \times 10^{-4}, \lambda_R = 0$	62.84	33.8	0.93	0.56	88.25

Bold values indicate the best performance in MSE

Table 2 Implementation for the L2-regularized FFD method

The L2-regularized FFD method	
Step 1:	Read the fixed image S and the moving image M
Step 2:	Use Gaussian smoothing, then conduct the affine transformation and return the parameters matrix
Step 3:	Set the parameters of the method, including the similarity measure, coefficients of L2 term and smooth term, initial grid spacing and the max B-spline levels.Assuming the max levels is m, then start the transformation:
	for i=1:1:m
	Make the initial grid of the ith level, calculate the similarity measure, transform the ith grid
	Optimize the energy function with L-BFGS algorithm until the minimum value is found
	Increase the resolution of grid, then conduct the transformation of the $i+1$th level
	end
	Transform the moving image with the best transformation grid found, and reconstruct the image by interpolation

For a better comparison, the methods mentioned, such as the classic FFD, Demons, Active Demons, MIAD, SIFT, SIFT-Demons and TV-L1, are also selected, and the parameters of all methods are set to get the best results, respectively.

4.1 Registration results of medical images

In this section, we used the liver MRI shown in Fig. 1 for non-rigid registration experiments to represent the medical image with large local deformation, which is different with rigid MRI method based on affine transformation [21].

The parameters of classic FFD and LFFD are set as follows. SAD is used as similarity measure, B-spline levels is 3, and initial spacing is 32×32. In the classic FFD, coefficient of smooth term is set to $\lambda = 10^{-2}$, while in LFFD, $\lambda_R = 5 \times 10^{-3}$ and coefficient of L2 term is set to $\lambda_L = 8 \times 10^{-4}$.

Figure 5 shows the registration results of liver MRI using the above methods. Figure 6 shows the difference between the fixed image and the registration results. Table 3 is the objective evaluation criteria.

After the analyzing of Figs. 5 and 6 and Table 3, we can draw a conclusion. The classic FFD method did well in the global transformation, but could not handle the strongly local deformation. The proposed LFFD solved the problems occurred in the classic FFD, while maintaining the good result of global transformation, and even had a better performance than TV-L1 in PSNR and MSE.

4.2 Registration results of DIR-Lab 4D CT datasets

Castillo and Castillo [22] have published 10 sets of lung 4D CT cases on the DIR-Lab website [23]. The images are marked by medical experts, and the mark points are used as the standard for evaluating the registration effect. Since the release of the datasets, a lot of scholars and researchers have used these datasets for evaluating various registration methods [22,24,25].

In the datasets, each set contained 10 images captured at different times from one patient, and the max expiratory phase and the max inspiratory phase image comprise 300 pairs of mark points. In Table 4, TRE (Target Registration Errors) means the average value of the distances between 300 pairs of mark points, and the data in parentheses are the standard deviation (STD).

In this section, we take the max expiratory phase and max inspiratory phase of the case1 for registration, then calculate the TRE and STD. For convenience, we take the registration

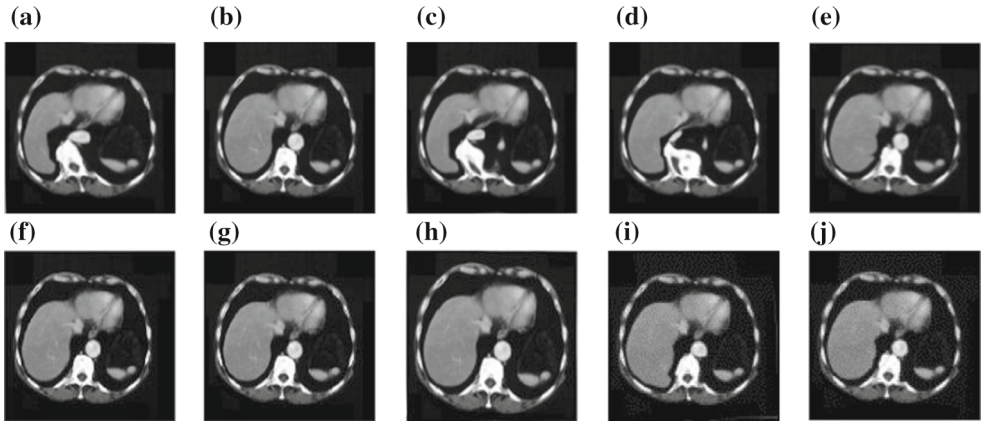

Fig. 5 Registration results of liver MRI. First row(from left to right): **a** moving image, **b** fixed image, **c** Demons, **d** AD, **e** MIAD; second row: **f** SIFT, **g** SIFT-Demons, **h** TV-L1, **i** FFD, **j** LFFD

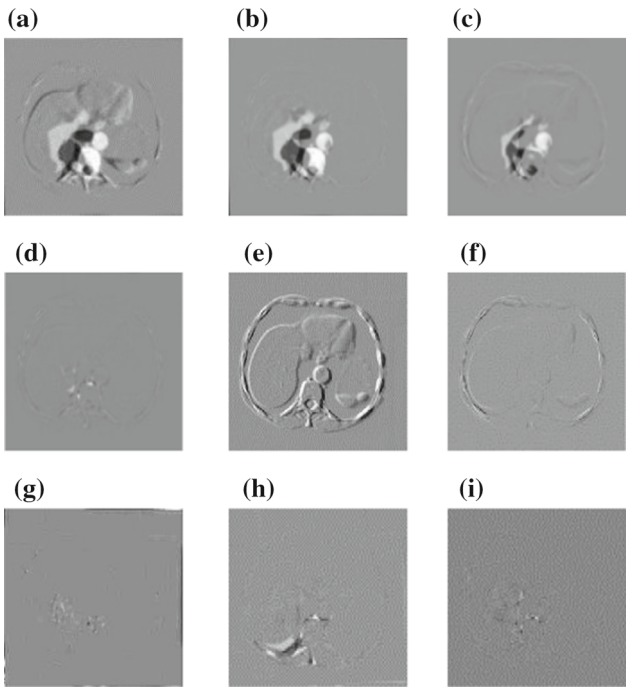

Fig. 6 Difference between the fixed image and the registration results. First row (from left to right): **a** Intial difference, **b** Demons, **c** AD; second row: **d** MIAD, **e** SIFT, **f** SIFT-Demons; third row: **g** TV-L1, **h** FFD, **i** LFFD

of case1 for a detailed description, and the parameters of classic FFD and LFFD are set to get the best registration results, respectively.

After numerous tests, the parameters of the two methods are set as follows. SAD is used as similarity measure, B-spline levels is 3, and initial spacing is $32 \times 32 \times 32$. In classic FFD, coefficient of smooth term is set to $\lambda = 10^{-4}$, while in LFFD, $\lambda_R = 6 \times 10^{-5}$ and coefficient of L2 term is set to $\lambda_L = 2 \times 10^{-5}$.

We captured the 30th, 50th and 70th slices in direction of axial for subjective evaluation, and the registration result can be seen in Fig. 7

To see from Figs. 7 to 8, for the 30th and 50th slices which have little difference with fixed images, the classic FFD and LFFD both achieve accurate registration. But when it comes to the 70th slices, which have big difference with fixed image, an over-registration appeared in the classic FFD as the red circle highlight in Fig. 8h. However, it is restrained in LFFD in Fig. 8i, and higher accuracy obtained.

Table 4 shows the TRE and STD after registration. It is clear that the LFFD achieved higher accuracy than the classic FFD. MLS is regarded as a baseline standard for measuring the validity of registration, and isoPTV has the best performance, which was published at the end of 2016. However, each of these methods to compare has some limitations on the application domain and cannot fit into any application data type. It is clear that the LFFD can improve the accuracy, and it is a relatively superior method, while it still has disadvantages compared to some methods. Although the LFFD uses all the pixels to conduct registration, it manipulates the control points, and then uses interpolation to estimate the displacement of all the pixels, rather than directly calculates. Therefore its accuracy is inferior to some publish methods. Besides, the LFFD has strong computational complexity and low efficiency in 3D image registration.

5 Conclusions

The comparative analysis of the above experiments show that the LFFD based on B-spline is a relatively effective registration method than the classic FFD. Meanwhile, this new method suppressed the over-fitting, well maintained the topologies and enhanced the robustness. Even though the efficiency is low when dealing with large datasets like 3D

Table 3 The objective evaluation criteria of the 8 methods

Methods	PSNR (dB)	MSE (10^{-5})	R_{cc}	MI	SSIM (%)
Before registration	62.53	3630	0.70	1.51	72.16
Demons	66.55	1440	0.79	1.65	83.88
AD	64.65	2220	0.88	1.71	89.27
MIAD	66.05	140	0.99	1.43	94.40
SIFT	63.52	2890	0.76	1.15	55.60
SIFT-Demons	**119.03**	**0.01**	**1.00**	**3.80**	**100.00**
TV-L1	77.56	110	0.99	2.90	98.75
FFD	70.77	540	0.95	1.66	84.82
LFFD	80.22	61.75	0.99	2.16	94.05

Bold values indicate the best performance in MSE

Table 4 The TRE and STD after registration using various methods

Case	TRE	MLS	CPP	4DLTM	isoPTV	FFD	LFFD
4DCT1	$3.89_{(2.8)}$	$1.58_{(1.30)}$	$1.07_{(1.10)}$	$0.97_{(1.02)}$	$\mathbf{0.76}_{(0.90)}$	$1.73_{(0.92)}$	$1.43_{(0.82)}$
4DCT2	$4.34_{(3.9)}$	$1.47_{(1.12)}$	$0.99_{(1.12)}$	$0.86_{(1.08)}$	$\mathbf{0.77}_{(0.89)}$	$1.82_{(1.13)}$	$1.53_{(1.08)}$
4DCT3	$6.94_{(4.0)}$	$2.27_{(1.40)}$	$1.23_{(1.32)}$	$1.01_{(1.17)}$	$\mathbf{0.90}_{(1.05)}$	$2.28_{(1.28)}$	$1.71_{(1.13)}$
4DCT4	$9.83_{(4.8)}$	$2.50_{(1.68)}$	$1.51_{(1.58)}$	$1.40_{(1.57)}$	$\mathbf{1.24}_{(1.29)}$	$2.46_{(1.55)}$	$2.02_{(1.32)}$
4DCT5	$7.48_{(5.5)}$	$2.55_{(1.92)}$	$1.95_{(2.02)}$	$1.67_{(1.79)}$	$\mathbf{1.12}_{(1.44)}$	$2.99_{(1.73)}$	$2.43_{(1.67)}$
4DCT6	$10.90_{(6.9)}$	…	$1.94_{(1.72)}$	$1.58_{(1.65)}$	$\mathbf{0.85}_{(0.89)}$	$3.18_{(1.77)}$	$2.47_{(1.50)}$
4DCT7	$11.00_{(7.4)}$	…	$1.79_{(1.46)}$	$1.46_{(1.29)}$	$\mathbf{0.80}_{(1.28)}$	$2.99_{(1.66)}$	$2.34_{(1.42)}$
4DCT8	$15.00_{(9.0)}$	…	$1.96_{(2.33)}$	$1.77_{(2.12)}$	$\mathbf{1.34}_{(1.93)}$	$3.10_{(2.44)}$	$2.58_{(2.04)}$
4DCT9	$7.92_{(3.9)}$	…	$1.33_{(1.17)}$	$1.19_{(1.12)}$	$\mathbf{0.92}_{(0.94)}$	$2.09_{(1.29)}$	$1.70_{(1.19)}$
4DCT10	$7.30_{(6.3)}$	…	$1.84_{(1.90)}$	$1.59_{(1.87)}$	$\mathbf{0.82}_{(0.89)}$	$2.62_{(2.20)}$	$2.16_{(1.81)}$

Bold values indicate the best performance with 4DCT datasets

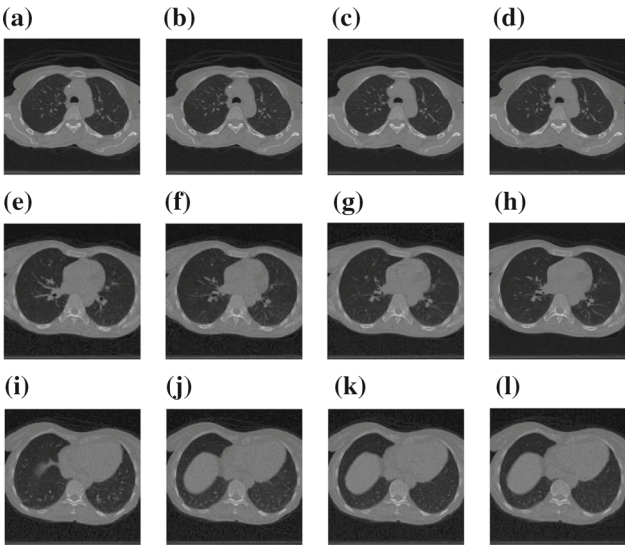

Fig. 7 The 1st column and the 2nd column show the moving images and fixed images, respectively. The 3rd column and 4th column show the captured images from registration result using classic FFD and LFFD, respectively. The 1st row to 3rd row correspond the 30th, 50th and 70th slices in direction of axial

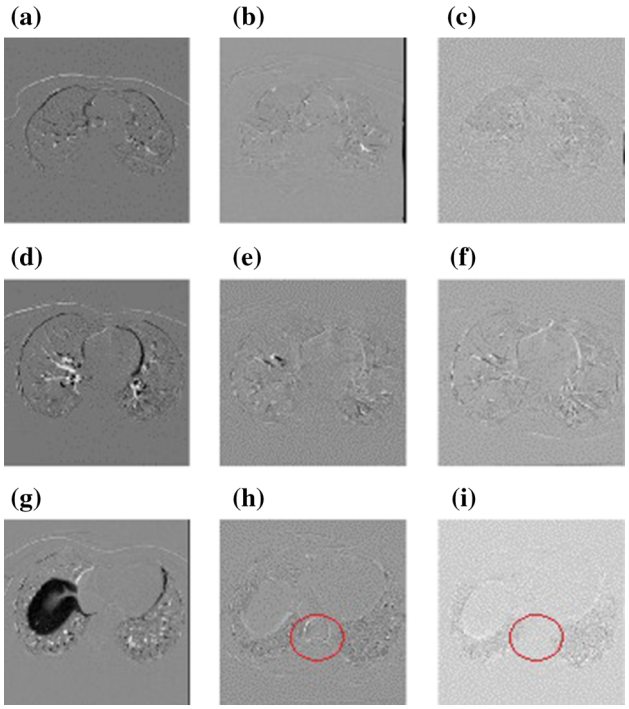

Fig. 8 The 1st column shows the initial difference images between moving images and fixed images, the 2nd column and the 3rd column show the difference between fixed images and corresponding slices from registration results using classic FFD and LFFD, respectively

images, we can handle this problem with GPU parallel computing methods. However, there are still some drawbacks. Firstly, it is not as good as isoPTV and other more advanced registration methods in the accuracy. Secondly, the coefficient of the L2 term is assigned with empirical value. These are new topics for our future research.

Acknowledgements This work was supported by National Natural Science Foundation of China (Nos. 81371635 and 81671848), Key Research and Development Project of Shandong Province (No. 2016GGX101017), and Research Fund for the Doctoral Program of Higher Education of China (20120131110062).

References

1. Zitov, Barbara, Flusser, Jan: Image registration methods: a survey. Image Vis. Comput. **21**(11), 9771000 (2003)
2. David, G.L.: Distinctive Image Features from Scale-Invariant Keypoints. Kluwer, Dordrecht (2004)
3. Du, S.: Scaling iterative closest point algorithm for registration of m–d point sets. J. Vis. Commun. Image Represent. **21**(56), 442–452 (2010)
4. Bay, H., Ess, A., Tuytelaars, T., Van Gool, L.: Speeded-up robust features. Comput. Vis. Image. Underst. **110**(3), 404–417 (2008)
5. Thirion, J.P.: Image matching as a diffusion process: an analogy with Maxwell's demons. Med. Image Anal. **2**(3), 243 (1998)
6. Wang, H., Dong, L.: Validation of an accelerated 'demons' algorithm for deformable image registration in radiation therapy. Phys. Med. Biol. **50**(12), 2887–2905 (2005)
7. Xue, P., Yang, P.: An effective non-rigid image registration method based on active demons algorithm. Acta Autom. Sin. **42**(9), 1389–1400 (2015)
8. Jia, D.: The Research of Non-rigid Registration Algorithm Based on Image Characteristics and Optical Flow. Master Thesis, ShanDong University
9. Pock, T., et al.: A duality based algorithm for TV- L, 1-optical-flow image registration. In: Medical Image Computing and Computer-Assisted Intervention - MICCAI 2007, pp. 511–518. Springer, Berlin, Heidelberg (2007)
10. Sun, D., Qiu, Z.: A new non-rigid image matching algorithm using thin-plate spline. Acta Electron. Sin. **30**(8), 1104–1107 (2002)
11. Rueckert, D., Sonoda, L.I.: Nonrigid registration using free-form deformations: application to breast MR images. IEEE Trans. Med. Imaging **18**(8), 712 (1999)
12. Wei, D.: Generalized sampling expansions with multiple sampling rates for lowpass and bandpass signals in the fractional fourier transform domain. IEEE Trans. Signal Process. **64**(18), 4861–4874 (2016)
13. Wei, D.: Reconstruction of multidimensional bandlimited signals from multichannel samples in linear canonical transform domain. Signal Process. IET **8**(6), 647–657 (2014)
14. Lee, S., Wolberg, G.: Scattered data interpolation with multilevel b-splines. IEEE Trans. Vis. Comput. Graph. **3**(3), 228–244 (1997)
15. Wei, D.: Image super-resolution reconstruction using the high-order derivative interpolation associated with fractional filter functions. IET Signal Process. **10**(9), 1052–1061 (2017)
16. Schnabel, J.A., Rueckert, D.: A generic framework for non-rigid registration based on non-uniform multi-level free-form deformations. In: International Conference on Medical Image Computing and Computer-Assisted Intervention, pp. 573–581 (2001)
17. Oliveira, F.P., Tavares, J.M.: Enhanced spatio-temporal alignment of plantar pressure image sequences using b-splines. Med. Biol. Eng. Comput. **51**(3), 267–276 (2013)
18. Neumaier, Arnold: Solving ill-conditioned and singular linear systems: a tutorial on regularization. SIAM Rev. **40**(3), 636–666 (1998)
19. Sun, D., Roth, S., Michael, J.B.: Secrets of optical flow estimation and their principles. In: Computer Vision and Pattern Recognition, pp. 2432–2439 (2010)
20. Zhang, S., Zhou, H.: Robust visual tracking using structurally random projection and weighted least squares. IEEE Trans. Circuits Syst. Video Technol. **25**(11), 1749–1760 (2015)
21. Song, H.: A parametric intensity-based 3d image registration method for magnetic resonance imaging. Signal Image Video Process. **11**(3), 455–462 (2017)
22. Castillo, R., Castillo, E.: A framework for evaluation of deformable image registration spatial accuracy using large landmark point sets. Phys. Med. Biol. **54**(7), 1849–1870 (2009)
23. https://www.dir-lab.com/
24. Castillo, E., Castillo, R.: Four-dimensional deformable image registration using trajectory modeling. Phys. Med. Biol. **55**(1), 305 (2010)
25. Vishnevskiy, V., Gass, T.: Isotropic total variation regularization of displacements in parametric image registration. IEEE Trans. Med. Imaging **PP**(99), 1-1 (2016)